Digital Holography on Moving Objects: Multiwavelength Height Measurements on Inclined Surfaces

Annelie Schiller[a], Tobias Beckmann[a], Markus Fratz[a], Dominik Belzer[a], Alexander Bertz[a], Daniel Carl[a], and Karsten Buse[a,b]

[a]Fraunhofer Institute for Physical Measurement Techniques IPM, Heidenhofstrasse 8, 79110 Freiburg, Germany
[b]Department of Microsystems Engineering, University of Freiburg, Georges-Köhler-Allee 102, 79110 Freiburg, Germany

ABSTRACT

Multiwavelength digital holography on moving objects enables fast and precise inline-measurements of surface profiles. Due to the use of multiple wavelengths, optically rough surfaces with structure heights in the micrometer range can be mapped unambiguously. In this work we explore the influence of the object velocity on height measurements on inclined surfaces. We show measurements using spatial-phase-shifting holography employing two wavelengths and object velocities of up to 90 mm/s with eye-safe cw-lasers with less than 1 mW of laser light. Despite motion blur exceeding the mean speckle size, reliable height measurements can be conducted at these velocities. The height map of a metal cone with two different slope angles (1 °, 10 °) is measured at an exposure time of 2 ms. Using line shaped illumination, each frame yields a height map of approximately 2×17 mm^2. The overlap between the frames allows averaging as the image is put together, improving data quality. The mean repeatability of the height information in the investigated setup is better than 4.5 µm at a synthetic wavelength of 214 µm.

Keywords: Digital holography, Holographic interferometry, Speckle interferometry, Speckle imaging, Height measurements. (8 keywords)

1. INTRODUCTION

Digital holography allows precise shape measurements of surfaces. The majority of industrial products are optically rough i.e. the roughness exceeds the visible wavelength. If such surfaces are illuminated by coherent light, random intensity patterns can be observed: speckle patterns.[1] Applying multiwavelength holography, reliable height data can be extracted out of these speckle patterns.[2] Furthermore, multiwavelength holography allows unambiguous measurement ranges from several micrometers to milimeters.[2–5] As holography is based on an interferometric principle, measurements are so far taken on stationary or quasi stationary objects.[2–7] However, measurements on moving objects would enable measuring large scale components without loss of resolution, just by moving the object along the sensor. In this case the measurement area in the direction of movement is limited only by the storage capacity of the computer. In order to understand the effect of object motion on the holographic measurement, the present work is conducted with two continuous wave lasers, exposure times of 2 ms and velocities up to 90 mm/s. This results in motion blur much larger than a mean speckle diameter, which is fundametaly different to the application of pulsed lasers.[6,7] The phase information of the object is extracted out of just one single camera frame by spatial phase shifting.[8] Height measurements of moving optically rough aluminum surfaces with inclination angles of 1 ° and 10 ° are shown. It is demonstrated that the geometric key parameters in the millimeter range can be measured with an accuracy smaller than 11 µm at an sampling pitch size of 11 µm, and a repeatability of the height information of less than 4.5 µm is achieved using a synthetic wavelength of 214 µm.

Further author information: (Send correspondence to Annelie Schiller)
Annelie Schiller: E-mail: Annelie.Schiller@ipm.fraunhofer.de, Telephone: +49 (0)761 8857 303

2. EXPERIMENTAL PROCEDURE

2.1 Setup

The experimental setup for spatial-phase-shifting multiwavelength holography is shown in Fig. 1 a). Two fiber-coupled external cavity diode lasers are used. Light at 632.66 and 634.54 nm is emitted, which results in a synthetic wavelength of 214 µm.[2] Polarization-maintaining fiber beam splitters split the light of each of the lasers into object and reference beam. In the object path, the two beams are combined by a fiber coupler to ensure that both waves have a common source point. The object beam is collimated by a spherical lens and focused using a cylindrical lens, so that the illuminated area (2×17 mm^2) on the object is much shorter along the direction of motion (x) than in the perpendicular direction (y). The light illuminating the object is convergent in x-direction and collimated in y-direction. The object is mounted on a stage, moving linearly in x-direction, i.e. perpendicularly to the optical axis. A fixed metal plate is mounted at the edge of the measurement area, serving as a stationary reference. The light scattered by the object passes the quarter wave plate twice, so the linear polarization is rotated by 90 ° and passes the polarizing beam splitter. A rectangular aperture limits the spatial frequencies reaching the camera. The larger side of the aperture (15 mm) is aligned perpendicular to the direction of movement (in y-direction), the shorter side (2.9 mm) is aligned in parallel to the direction of motion. Consequently the speckles are smaller in y-direction and larger in x-direction. This results in a lower resolution in the direction of motion, where motion blur occurs anyway. A single lens (f=100 mm) behind the aperture images the object onto the camera, where the light is superimposed with the reference beams. A polarizer in front of the camera enables interference of reference and object beams. Both reference beams are tilted to the optical axis by θ_1 and θ_2 to achieve spatial phase shifting. The end of each fiber is placed in the same distance to the camera as the aperture. Due to that a single spatial carrier frequency is achieved.[9] A sequence of camera frames is acquired with an exposure time of 2 ms while the object is moved continuously in x-direction. The frame rate of the camera is chosen such that the object moves 0.2 mm between the single frames, which equals 54 px on the camera image. In order to measure the whole sample, 91 frames are acquired at each velocity.

In order to examine inclined surfaces a sample cone was measured. A sketch of its geometry is shown in Fig. 1 b). It consists of an inner cone with a slope angle $\alpha_1 = 1\,°$ and an attached truncated cone with a slope angle of $\alpha_2 = 10\,°$. The radius of the intersection of the two cones (r_t) is at an height of z_t. This cone is produced out of aluminum by turning.

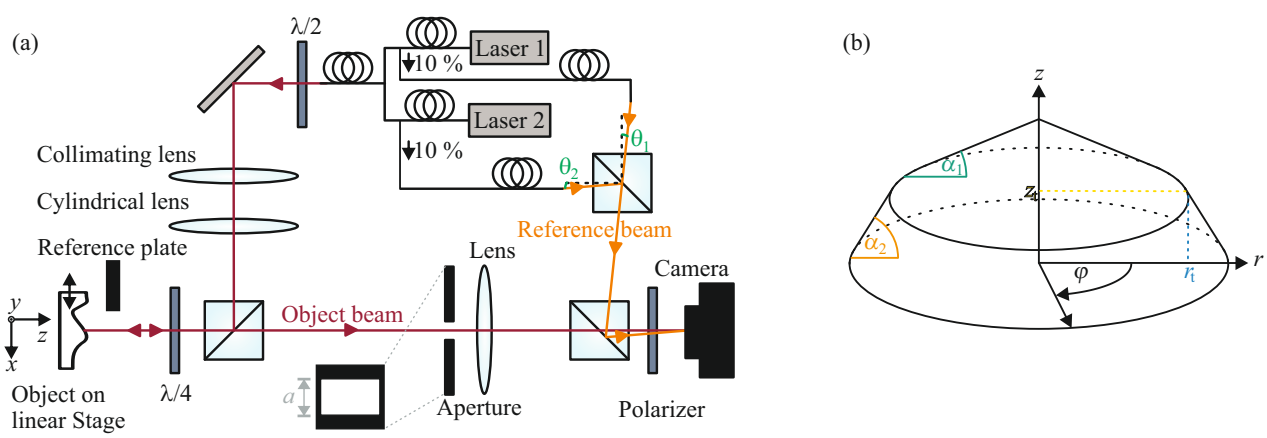

Figure 1. a) Experimental setup for spatial-phase-shifting two-wavelength holography with an object moving continuously in x-direction. The laser light is split into object beam and reference beam. The reference beam is tilted to the optical axis to achieve spatial phase shifting. The object beam scattered by the object passes a rectangular aperture resulting in a speckle pattern with smaller speckles in y- and larger speckles in x-direction. b) Truncated cone with a cone on top, having two slope angles α_1 and α_2. The transition point between the two cones is at radius r_t and height z_t.

2.2 Data Processing

The single camera frames (5120 px × 256 px, 10 bit) are processed individually and consequently overlaid and averaged. The raw image (Fig. 2 a)) is Fourier transformed (see Fig. 2 b)). In the Fourier image, the DC term can be seen in the center. The interference terms are aligned symmetrically. The position of theses side bands are determined by the tilt angles θ_1 and θ_2, which are adjusted such that the side bands do not overlap. For each of the two wavelengths one side band is cropped out (indicated by the red rectangles in Fig. 2 b)) and shifted to the center. The inverse Fourier transform of each cropped region results in a complex-valued image containing the information of one wavelength λ.[9] The phase map for one wavelength (Fig. 2 c)) shows a random phase distribution due to the surface roughness of the object. The phase difference for the two single wavelengths equals the phase of the synthetic wavelength $\Lambda = \lambda_1\lambda_2/|\lambda_1 - \lambda_2|$ (see Fig. 2 d)).[2] An efficient way to calculate this phase difference is evaluating the product of the complex image of one wavelength and the complex conjugated image of the other wavelength, resulting in the image for the synthetic wavelength. The complex image of the synthetic wavelength is processed further. An inclined plane is subtracted to eliminate the phase tilt due to misalignment. This correction is identical for all frames. To decrease the size of the resulting complex image, the single frames are downsampled by a factor of 3 and filtered with a filter kernel of 3 px × 3 px afterwards.

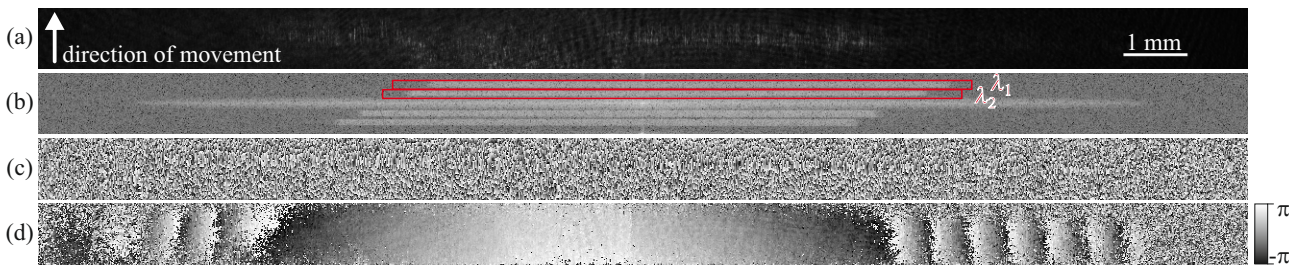

Figure 2. Data processing steps of one single raw image are shown: The raw image (a) is Fourier transformed (b). For each wavelength, the first diffraction order (red rectangle) is cropped, shifted to the center, and the reverse Fourier transform is calculated. Out of that the phase map of one single wavelength (c) can be calculated. The phase map of the synthetic wavelength is shown in (d).

An offset is added to the phase values of every frame, to achieve the same phase value of the reference plate in every frame, correcting phase drifts during acquisition of the image sequence. Subsequently the overlapping sections of the single frames are averaged, weighted by the amplitudes of every pixel in the complex image. This results in an expanded image in x-direction showing the whole object. The consequent phase map is corrected by subtracting a parabolic cylinder curved in the y-direction in order to eliminate the aberrations of the lens and the misalignment of the setup. The parameters for this correction are determined by taking data for a plane object.

The height h of every pixel of an object can be calculated out of the phase value ϕ by $h = \Lambda\phi/(4\pi)$. The height of the cone exceeds the unambiguous measurement range of the wavelengths used. Thus the height data is unwrapped.[10]

The resulting height map is evaluated to analyze the key parameters of the sample object (Fig. 1 b)). Therefore the cone is divided into 37 radial slices enclosing all the same angle of 9.73 °, starting in the center of the cone. The height values are averaged over every slice and two lines are fitted to the data. This is shown in Fig. 3, where the cone is divided in 8 slices (a) and the mean height of the green slice is plotted versus the radius (b). Out of the slope of the two lines, the inclination angle of each of the two sections of the cone can be calculated. The intersection of the two lines gives the height z_t and radius r_t of the transition circle of the two cones.

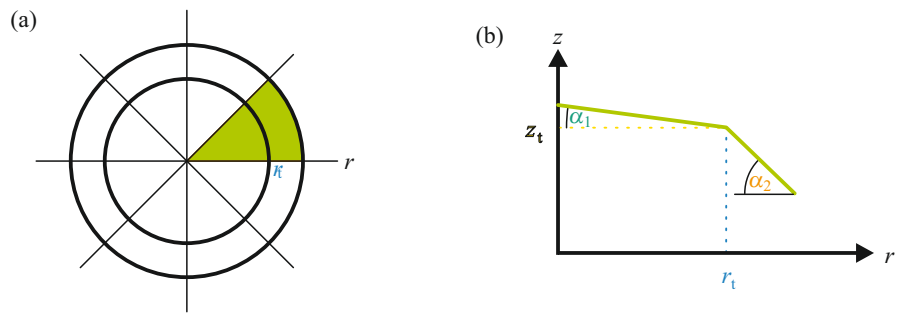

Figure 3. Sketch of the cone, which is divided into 8 radial slices (a). The averaged data of the green slice is shown in (b).

3. RESULTS

3.1 Height measurement

Exemplarily the height map of the unwrapped cone moving with 10 mm/s is depicted in Fig 4. This velocity equals an acquisition data rate of 14 MPx/s, or 1.5 MPx/s in the downsampled case. Moving the cone with 90 mm/s requires a data rate of 130 MPx/s, or 15 Mpx/s in the downsampled case. A small defect on the surface can be seen clearly (black rectangle). The shape of that defect is shown in a magnified 3D view in Fig. 4.

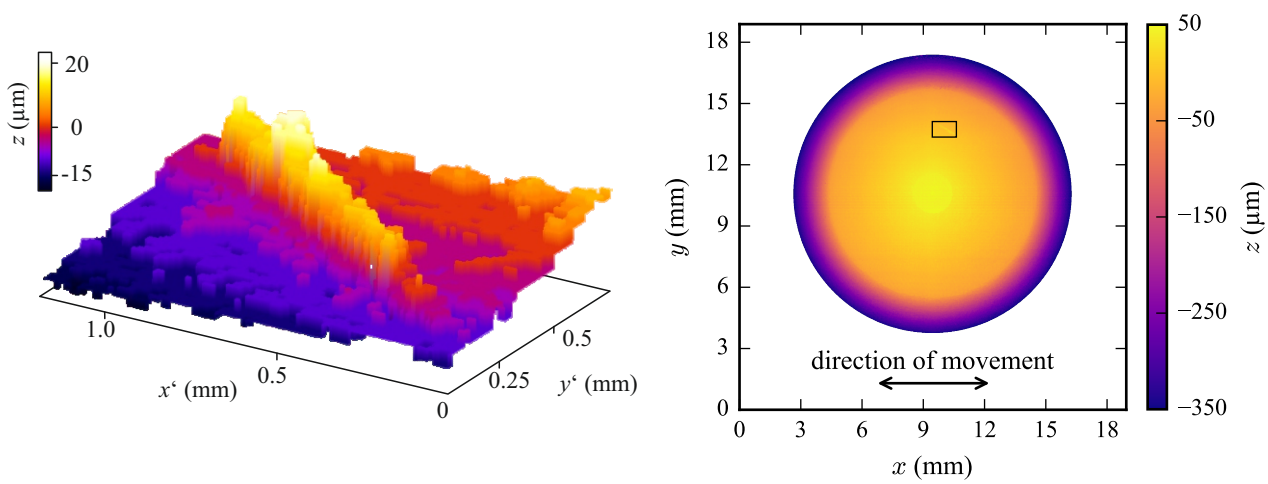

Figure 4. Unwrapped height map of the sample cone moving with 10 mm/s. Magnified 3D view of the defect in the black rectangle is shown.

In order to measure the repeatability of this method, 10 measurements were conducted at each velocity. Each pixel of the downsampled height map represents one height value. The standard deviation of every downsampled pixel in the height map is calculated. The mean standard deviation versus velocity is shown in Fig. 5. An increasing deviation with higher velocities is observed. The lowest deviation is $\sigma = 1.2$ µm at 2 mm/s, the highest deviation is $\sigma = 4.5$ µm at 90 mm/s.

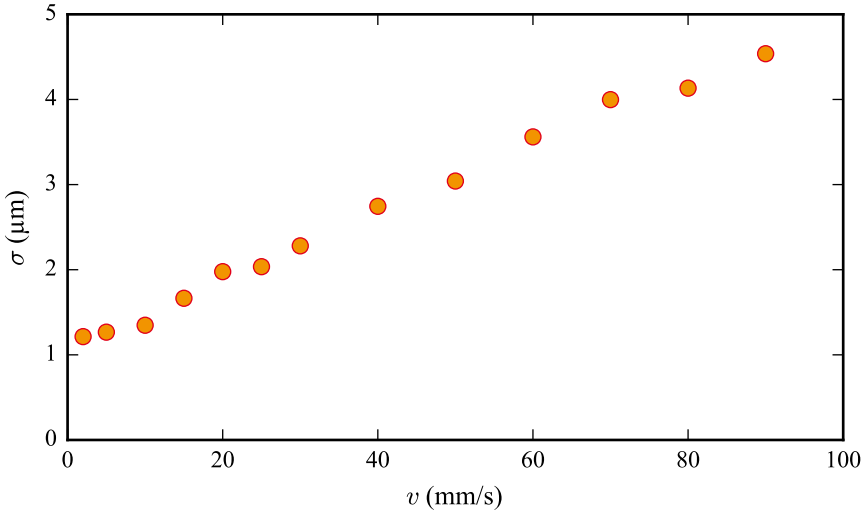

Figure 5. Mean standard deviation of the height map of one downsampled pixel of 10 measurements averaged over the whole image.

3.2 Geometric features

Analyzing the two line fits for every slice of the cone and averaging them results in the key parameters and their standard deviation, which are depicted in Fig 6. The slope angles α_1 and α_2 can be determined precisely up to a velocity of 90 mm/s with σ_α smaller than 0.1 °. Despite the motion blur of 180 µm at an velocity of 90 mm/s and an exposure time of 2 ms, the base radius r_t = 5 mm can be determined within σ = 11 µm. Considering that one pixel in the downsampled image represents 11 µm on the object, this deviation equals the lateral resolution. The transition height z_t = -53 µm is measured with σ smaller than 2 µm nearly independently of the object velocity.

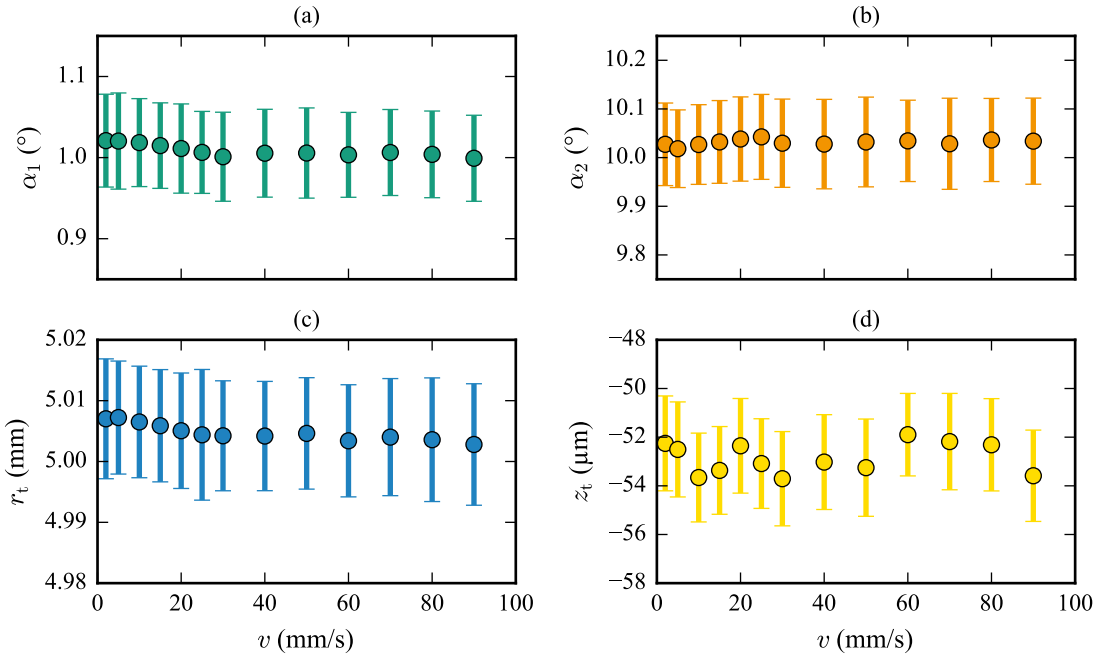

Figure 6. Mean measurement results and its standard deviations of the key parameters: the slope angles α_1 (a) and α_2 (b), the radius r_t (c) and the transition height z_t (d) dependent on the velocity calculated out of 37 radial slices of the cone.

Averaging all 37 slices of one cone yields an average cone geometry for every cone measurement. The height deviation to this geometry is depicted in Fig. 7, in order to demonstrate that inclined surfaces can be measured independently of their alignment towards the direction of movement. On the left the deviation data for a cone moving with 10 mm/s is shown and on the right results for a cone moving with 90 mm/s are presented. These deviations include not only measurement errors but also irregularities of the sample shape like the defect shown in Fig. 4 and synchronization errors between the linear stage and the camera. Consequently these deviations are expected to be larger or equal to those shown in Fig. 5. The measurement of the cone moving with 10 mm/s differs with $\sigma = 4.9$ µm from the average cone. The deviation of the cone moving with 90 mm/s is higher with $\sigma = 11.7$ µm. The outer area of the cone with a higher slope (α_2), moving with 90 mm/s, shows higher deviations. Nevertheless these results prove that surfaces with inclination angles of 1 ° and 10 ° can be measured independently of their alignment towards the direction of movement with an accuracy in the micrometer range.

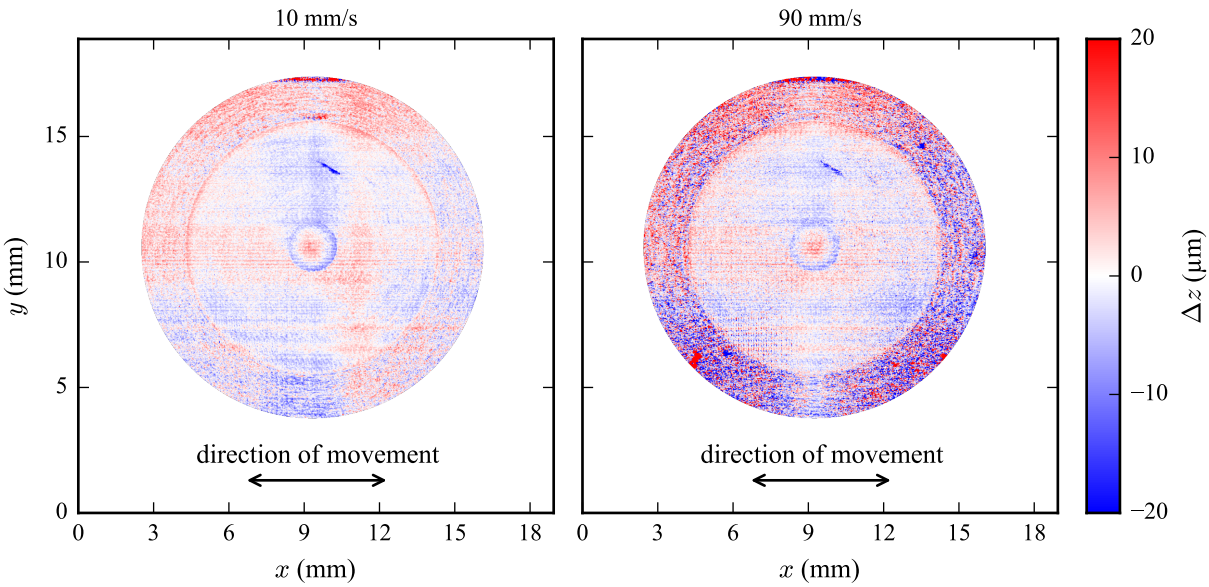

Figure 7. Height difference between the data taken from a single measurement and the real-shape profile for the sample cone measured at 10 mm/s and 90 mm/s leading to a deviation of $\sigma = 4.9$ µm at 10 mm/s and $\sigma = 11.7$ µm at 90 mm/s, respectively.

4. CONCLUSION

We have demonstrated two-wavelength holography using spatial phase shifting with a cone as a test object moving with velocities of up to 90 mm/s. Two wavelengths of 632.66 and 634.54 nm were used, which results in a synthetic wavelength of 214 µm. At each velocity, a set of 91 frames was acquired. Those frames were processed in order to get an expanded field of view in the direction of motion. The complete cone profile with two adjacent surfaces with slope angles of 1 ° and 10 ° could be measured with standard deviations smaller than 0.1 ° for every velocity. The 5 mm radius could be determined within 1σ of 11 µm. The difference of one height measurement to the averaged geometry for the sample cone leads to a deviation of $\sigma = 4.9$ µm at 10 mm/s and $\sigma = 11.7$ µm at 90 mm/s, respectively. The repeatability of the downsampled height map is 4.5 µm per pixel. These presented measurements show that moving inclined surfaces can be measured with a high precision despite motion blur.

REFERENCES

[1] Goodman, J. W., "Some fundamental properties of speckle," *Journal of the Optical Society of America* **66**(11), 1145–1150 (1976).

[2] Wagner, C., Osten, W., and Seebacher, S., "Direct shape measurement by digital wavefront reconstruction and multiwavelength contouring," *Optical Engineering* **39**(1), 79–85 (2000).

[3] Mann, C. J., Bingham, P. R., Paquit, V. C., and Tobin, K. W., "Quantitative phase imaging by three-wavelength digital holography," *Optics Express* **16**(13), 9753–9764 (2008).

[4] Carl, D., Fratz, M., Pfeifer, M., Giel, D. M., and Höfler, H., "Multiwavelength digital holography with autocalibration of phase shifts and artificial wavelengths," *Applied Optics* **48**(34), H1–8 (2009).

[5] Fratz, M. and Carl, D., "Novel industry ready sensors for shape measurement based on multi wavelength digital holography," in [*Fringe 2013*], Osten, W., ed., 479–484, Springer Berlin Heidelberg, Berlin, Heidelberg and s.l. (2014).

[6] Pedrini, G., Fröning, P., Tiziani, H. J., and Gusev, M. E., "Pulsed digital holography for high-speed contouring that uses a two-wavelength method," *Applied Optics* **38**(16), 3460–3467 (1999).

[7] Tian, L., Loomis, N., Dominguez-Caballero, J. A., and Barbastathis, G., "Quantitative measurement of size and three-dimensional position of fast-moving bubbles in air-water mixture flows using digital holography," *Applied Optics* **49**(9), 1549–1554 (2010).

[8] Ichioka, Y. and Inuiya, M., "Direct phase detecting system," *Applied Optics* **11**(7), 1507–1514 (1972).

[9] Saldner, H. O., Molin, N. E., and Stetson, K. A., "Fourier-transform evaluation of phase data in spatially phase-biased tv holograms," *Applied Optics* **35**(2), 332–336 (1996).

[10] Goldstein, R. M., Zebker, H. A., and Werner, C. L., "Satellite radar interferometry: Two-dimensional phase unwrapping," *Radio Science* **23**(4), 713–720 (1988).